

P6.6 NEAR REAL TIME MEASUREMENT OF SEA-SALT AEROSOL DURING THE SEAS CAMPAIGN: COMPARISON OF EMISSION BASED SODIUM DETECTION WITH AN AEROSOL VOLATILITY TECHNIQUE*

A.J. Hynes[†], P. Campuzano-Jost, H. Maring
Division of Marine and Atmospheric Chemistry, RSMAS, University of Miami, Miami, FL

C.D. Clark
Department of Environmental and Chemical Sciences, Chapman University, Orange, CA

D. S. Covert
Department of Atmospheric Sciences, University of Washington, Seattle, WA

S. Howell, V. Kapustin, A. Clarke
University of Hawaii, Honolulu, HI

E. S. Saltzman
University of California at Irvine, Irvine, CA

1. INTRODUCTION

It is clear that attempts to better understand and quantify both the direct and indirect forcing effects of atmospheric aerosols have changed our view of their role in climate change (Prospero, 2002). While many early studies focused exclusively on sulfate aerosols (Charlson et al., 1992), it is now clear that sea salt, mineral dust and organic aerosols play a significant effect in direct scattering of solar radiation (Piliinis et al., 1995, Satheesh et al., 1999). Initial studies of the indirect effects of forcing via their impact on cloud formation and cloud droplet size distribution again focused on sulfate aerosol based on the assumption that this was the dominant source of cloud condensation nuclei (CCN) in the marine boundary layer (Charlson et al., 1987). In recent years this view has been challenged and the potential role of sea salt and organic compounds has been a subject of several investigations. An early study using electron microscopy identified submicron sea salt particles in membrane filter samples based on its cubic structure (Meszaros et al., 1974). A number of subsequent studies used more direct techniques and found the fraction of submicron sea salt to be extremely small. Radke and Hobbs (1969) used a flame emission instrument to simultaneously measure altitude profiles of CCN and sodium containing particles in the Olympic Mountains in Washington State. They concluded that the Pacific Ocean was the main source of sodium containing particles, but these constituted less than 1% of the

active CCN. A similar study by Hobbs (1971) over the Pacific Ocean sampled between sea level and 10,000 ft and again concluded that less than 1% of the active CCN contained sodium.

In more recent work, O'Dowd and coworkers (1993, 1997) have presented a rather different view based on measurements obtained using aerosol volatility techniques. They suggested that sea salt aerosol can provide the primary source of CCN, even under sulfate rich conditions. One of the problems in assessing the relative roles of sea salt and sulfate aerosol is related to the difficulty of measuring in-situ "chemically resolved" aerosol size distributions. The physical and chemical properties of aerosols are extremely variable and much of the current, very limited database was obtained with indirect measurements. One approach, developed by Clarke and coworkers (1991, 1993) uses aerosol volatility to distinguish between sea salt and sulfate aerosols.

Direct measurements of size segregated individual aerosol particles using laser ablation coupled with analysis by time-of-flight mass spectrometry provide contrasting results. Measurements at Cape Grim during the ACE-1 experiment reported that almost all aerosols larger than the 0.13 μm instrument detection limit contained some sea-salt (Murphy et al., 1998). In contrast, measurements during the INDOEX campaign employed a similar technique and found little sea-salt contribution to the submicron aerosol (Guazzotti et al., 2001). Both sampled clean air but with a significant difference in the wind speed and hence the sea salt environment. Laser ablation coupled with mass spectrometry provides a powerful tool for analysis of single particles, however it is a semi-quantitative technique. In this work we describe the field deployment of instrumentation which is

* This extended abstract has been submitted to the Journal of Atmospheric and Oceanic Technology.

[†] RSMAS/MAC, University of Miami, 4600 Rickenbacker Causeway, Miami, FL 33149, [email: ahynes@rsmas.miami.edu](mailto:ahynes@rsmas.miami.edu)

designed to provide quantitative, rapid, near real time analysis of the sodium content of marine aerosols in an effort to resolve some of these issues.

The SEAS deployment offered the opportunity to compare this method with measurements that used aerosol volatility techniques coupled with optical particle counting to infer sea-salt size distributions. The campaign took place from April 16 to May 1, 2000 at Bellows AFB on the east side of Oahu, where the University of Hawaii Department of Oceanography maintains a tower for aerosol measurements (cf. Clarke et al, this issue).

2. INSTRUMENTATION

The basic design and calibration of the aerosol sodium detector (ASD) was described by Clark et al., (2001) and contains a schematic of the instrument.

The basic principle of operation of the ASD is the volatilization of aerosol particles in a high temperature flame, atomization of the sodium salts to give sodium atoms and detection of the emission at 589.0 (D_2 line) and 589.6 nm (D_1 line) from thermally excited sodium atoms. The ASD consists of an aerosol sampling and injection system to introduce aerosol particles into the flame, a pre-mixed laminar hydrogen/air flame for volatilization of the aerosol and atomization of sodium salts, and PMTs (photomultiplier tubes) that detect the emission and associated electronics for data acquisition. It is possible to monitor size resolved aerosols by sampling through a differential mobility analyzer. The field instrument deployed in the SEAS campaign was a ruggedized, improved version of the ASD described previously, modified to employ a 50% larger sampling volume. In addition, a smaller burner head allowed for faster flame velocities, attaining higher flame temperatures, while reducing total gas consumption. Entrainment of sodium aerosols from the surrounding air into the ASD flame was particularly troublesome in the trailer in which the ASD was located at the SEAS site. In order to discriminate against coincidental or spurious aerosols from around the burner, a makeshift aluminum chimney was constructed on site. This shielded the flame quite effectively, but ~1% of the sample could be identified as entrained laboratory particles.

As the instrument's probed quantity is mass, a large dynamic range is needed to cover the aerosol size range of interest. By combining three PMTs with different gain settings, we achieved a dynamic range of about 2000 (180 to 2300 nm equivalent dry NaCl diameter). The detection volume in this configuration is better defined, improving discrimination against spurious aerosol events. Fig. 1 shows the correlation

between the three PMTs for a typical emission data set taken at SEAS. For all measurements during SEAS the differential mobility analyzer was not used to select a particular size aerosol thus the ASD sampled the aerosol size distribution transmitted by the inlet system. Hence we measure a distribution of emission signals that are proportional to the sodium content of the aerosol particle. However we have no information on the actual mass of the particle that produced the emission signal. The emission signals are converted to an absolute sodium mass using the calibration procedure described below and size distributions are obtained by converting sodium mass to an equivalent volume of "dry sodium chloride" based on an assumed density.

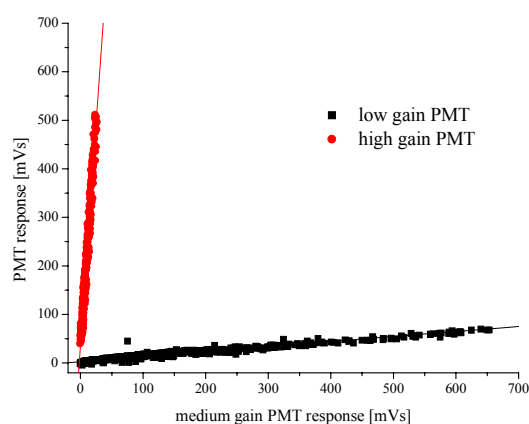


Figure 1: Correlations of the signal response of the three detectors for one typical SEAS sample.

2.1. Calibration:

The ASD is calibrated with monodisperse aerosols of known sizes, produced by a VOAG (vibrating orifice aerosol generator) (TSI Mod. 3050, (Berglund, 1973)). The VOAG produces aerosol particles with a known sodium content providing an absolute calibration standard for the emission signal. In a variety of tests described previously (Clark et al., 2001) we found that ASD emission signals were linear, increasing with increasing sodium concentration as expected. A linear response of the ASD to variation in droplet sodium concentration demonstrates that we are able to reproducibly vary the initial droplet sodium concentration, volatilization of the aerosols is complete and independent of sodium concentration and that the flame remains optically thin. In addition we demonstrated the absence of any chemical interference effects.

The instrument underwent an extensive recalibration after the completion of the SEAS campaign that addressed issues relating to absolute

calibration, transmission and data acquisition. Generation of well-defined monodisperse aerosol particles of variable sodium concentration is critical for ASD calibration. The initial size of the droplet as a geometric diameter produced by the VOAG can be calculated from (Westenberg, 1990):

$$D_d = \sqrt[3]{\frac{6Q}{\pi f}} \quad (1)$$

where f is the frequency of orifice vibration (s), Q is the liquid flow rate (cm^3/s) and D_d is the droplet diameter (cm). The absolute amount of sodium is calculated from the droplet volume and solution concentration. It does not however validate the absolute concentration calibration since an error in the droplet size calibration will produce a linear response but an error in the absolute concentration.

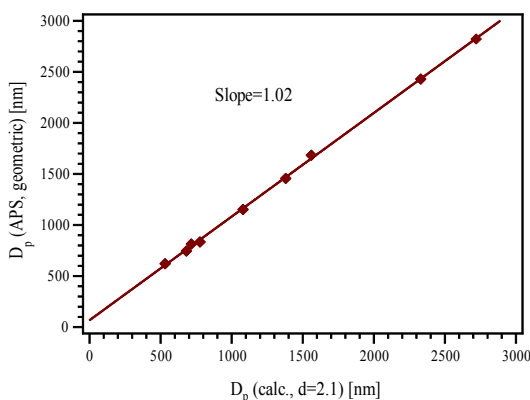


Figure 2: Correlation between calculated dry sizes for VOAG generated aerosols and the sizes measured with the APS, assuming dry aerosols.

To increase reproducibility of the VOAG aerosol output, a He-Ne laser beam was focused on the liquid jet, about 8 mm downstream from the vibrating orifice, and the absorption pattern monitored with a photodiode, allowing the droplet breakup process to be monitored in real time. Under correct operation a uniform absorption trace was observed with a frequency that matched the driving frequency of the VOAG crystal. All calibration experiments were performed while simultaneously monitoring the droplet size. The VOAG drying tube was modified to run at very high dilution flows and hence low relative humidity (RH). It was possible to reach RH as low as 20% under these conditions. In order to achieve good counting statistics, actual calibrations were taken at a RH of 45 to 50%. Provided the absorption trace is clean, the output of the VOAG is always monodisperse. Under these conditions we monitored the sodium emission signal as a function of sodium concentration. Fig.2 shows the relative emission

signal for all three PMTs, normalized to the sensitivity of the highest gain PMT and plotted against the calculated dry mass of sodium. The linearity over almost 3 orders of magnitude is quite remarkable. Standard errors were in the range of 3%, but are mainly caused by the width of the “monodisperse” VOAG distribution.

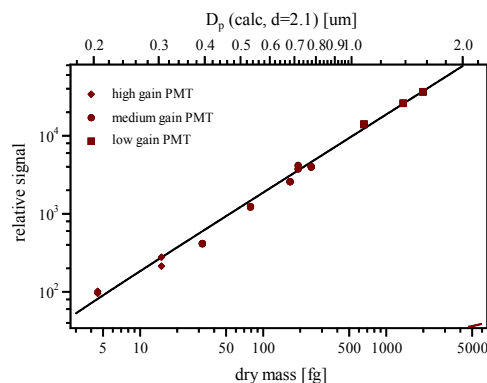


Figure 3: 11 point calibration of the ASD over the dynamic range of the three photomultipliers, normalized to the response of the highest gain detector. Both dry NaCl mass and calculated diameter (for a dry density of 2.1) of the synthetic aerosols are plotted

As noted above this demonstrates the linearity of the detection but does not validate the absolute mass calibration since errors in the calculation of droplet volume would produce a linear response. To ensure that the initial droplet volume calculation was correct, we attempted to completely dry the aerosols and compare the calculated and measured particle sizes. Fig. 3 shows the correlation of the calculated VOAG aerosol sizes with the actual sizes measured with an Aerosol Particle Sizer (APS, TSI Mod. 3310). The aerodynamic particle sizes measured by the APS were corrected to give geometric diameters assuming spherical particles, theoretical sizes were calculated, assuming the density of the aerosol to be that of pure seasalt, 2.1 g/cm^3 (Tang, 1997). The measured particle sizes agree well with those calculated assuming dry seasalt. As a result of these measurements we discovered that our original SEAS calibration, and hence a preliminary report of a SEAS distribution (Clark et al, 2001) was in error by a factor of 2 in mass. Since a cubic factor relates mass and diameter, the reported distribution, given as an equivalent dry NaCl diameter, has calculated diameters that are a factor of 1.3 too low. As noted in the paper, this distribution was not corrected for transmission efficiency through the ASD.

The strong correlation of calculated and theoretical diameters independent of size and sizing instrument gives us confidence that our current

absolute calibration is accurate. Thus we can extrapolate a theoretical detection limit of the ASD of around 150 nm in equivalent dry NaCl diameter. The current operational detection limit is set by the need to reliably trigger the data acquisition sequence off an emission event. At SEAS it was necessary to raise the triggering threshold for the acquisition electronics in order to discriminate against small room aerosols as well as false triggers and the operational detection limit was around 200 nm in equivalent dry NaCl diameter.

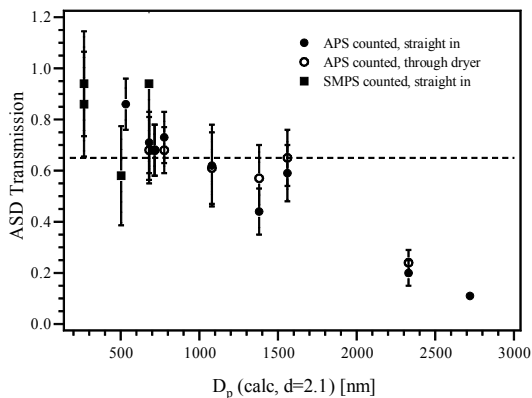


Figure 4: Transmission efficiencies of the ASD for different sizes, categorized by counting method. Also, for some sizes, the efficiency of aerosols dried through the nafion dryer is shown. The black dotted line shows the average value used for analysis of the SEAS data.

2.2. Transmission efficiency

The transmission efficiency of the ASD was determined as a function of particle diameter by sampling monodisperse VOAG particles of various diameters and comparing the ASD count rate per cycle with the measured particle number density. Small particles were passed through a DMA (TSI Mod. 3081) set at the maximum of the distribution and measurements were taken at the output with both the ASD and a condensation particle counter. Most VOAG particles are multiply charged, so transmission through the DMA was low and counting statistics were poor. Particles above 900 nm were measured with the APS and ASD in similar plumbing configurations. Fig. 4 summarizes the measured transmission ratios.

Overall, transmission is fairly constant between 500 and 2000 nm, perhaps increasing slightly below 500 nm. The fall off between 2000 nm and 3000 nm is to be expected from the deposition velocities for such aerosols in our injection volume (84 cm long, 7.1 mm id, 16 s residence time). Transmission was measured through a nafion with similar results. For the analysis of the SEAS data, an average value of

65% was taken, so that absolute number concentrations at the edges of the distribution might be systematically too low or too high.

3. SAMPLING CONFIGURATION AT SEAS.

Aerosols were sampled at the tower at Bellows at a height of 12 m above sea level. The inlet used in this study was a 3/8" ID black carbon rich silicone tube pointing into the wind, drawing 11 l min⁻¹, of which 0.4 l were dried through a 60 cm long 1/4" steel nafion dryer (Permapure Inc., Mod. MD-24) and drawn into the ASD. The actual sampling velocity at the top of the inlet was 2.5 m/s. At typical wind speeds of 6-8 m/s, such an inlet should slightly over-sample big particles. As the ASD is not designed for detection of particles > 3 μm aerodynamic diameter, over-sampling should not be a concern as long as there were no other losses.

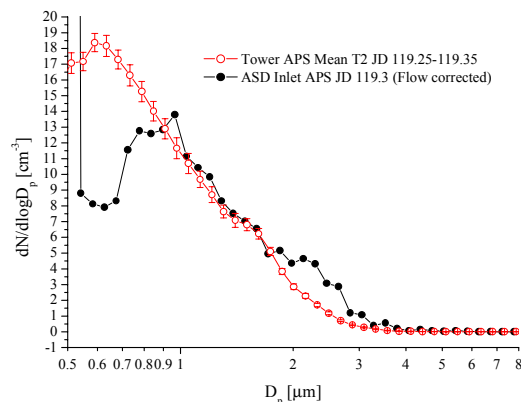


Figure 5: Comparison of data taken with an APS at the ASD inlet injection loop (sampling from tower) with an APS located on the sampling tower, 2 m below the ASD sampling inlet. Aerodynamic diameters are shown.

Some tests were run in order to validate the inlet transmission. On two different days, an SMPS and an APS were set up to sample the air going into the ASD injection loop. These measurements were compared to coincident aerosol measurements using an APS on the sampling tower (Clarke et al. this issue). The inlet for the aerosol instruments was 2 m below the inlet for the ASD. Fig.5 compares the data from the APS at the ASD injection loop with APS measurements taken on the tower. In the range above 1 μm diameter where the APS performs most reliably, the agreement between the tower APS and the injection loop APS is excellent up to 2 μm. Beyond 2 μm, the injection loop APS measurements were higher than the tower APS measurements but this might be caused by poor counting statistics since the injection loop APS sampling period was six

times shorter than that of the tower APS.

Fig. 6 compares Scanning Mobility Particle Sizer (SMPS, TSI Mod. 3936) measurements at the injection loop with tower measurements. The agreement is satisfactory, so over-sampling and diffusional losses were probably not an issue in this region. We conclude our inlet provided a representative sample of outside air for particles between 100 nm and 2 μm diameter.

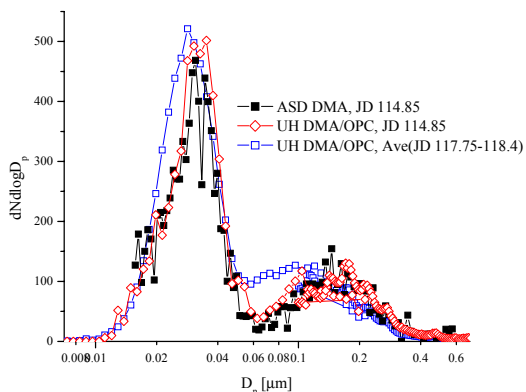


Figure 6: As Figure 5, but comparing data taken with our SMPS through our inlet with UH's data. Also shown is the average of UH's data during our first 24 h measurement period.

4. RESULTS

4.1. Timeframe

The ASD operated continuously for two 24 h periods, one starting at 11:00 am local time on 4/26/00 and the other at 11:00 am local time on 4/28/00 (JD 117.875-118.875 and JD 119.875-JD 120.875, respectively). Samples were taken on a two minute cycle time which consisted of one minute for sampling and one minute for analysis. Each sample gave 50-100 sodium signals. To improve counting statistics, ten injection cycles were combined, giving an effective time resolution of 20 min.

During JD 118 a front came over Bellows Beach (Clarke et al (this issue)), and from the second part of that day the origin of the airmass changed, although local conditions such as wind and humidity remained unchanged. Accordingly we measured both undisturbed marine as well as post-frontal aerosol.

4.2. Analysis

Instrumental problems precluded analysis of three hours of data from the first day of measurements. All other data sets were analyzed using the corrected calibrations taken on JD 119 and

JD 121. As stated, the gain ratios calculated from the photomultiplier correlations in each data set were stable within 10% over the course of the two days, as shown in Fig. 1. There was a small long term drift on the order of 5% in the sodium mass calibration, probably due to small instabilities in flame flow or warming of the photodetectors and the calculated equivalent NaCl diameters were corrected for this.

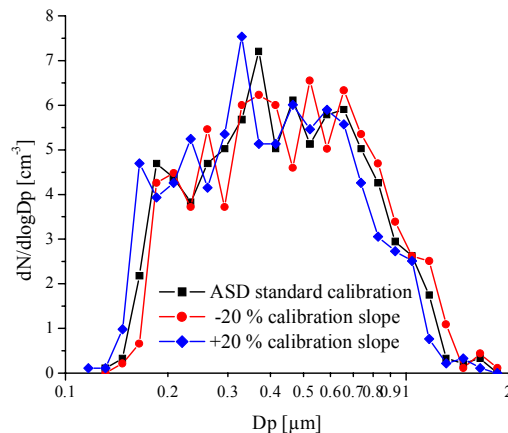


Figure 7: Typical sodium size distribution for the second day of measurements (JD 120) showing the effect of the 20% mass calibration uncertainty on size.

Each emission signal was inspected prior to integration, in order to discriminate against coincidental or spurious aerosols from around the burner. As noted above ~1% of the sample could be identified as contaminate particles based on the shape of the emission traces and the correlation between the PMT signals. Very small emission signals with doubtful traces were discarded, which might have resulted in our undercounting at or near the detection limit.

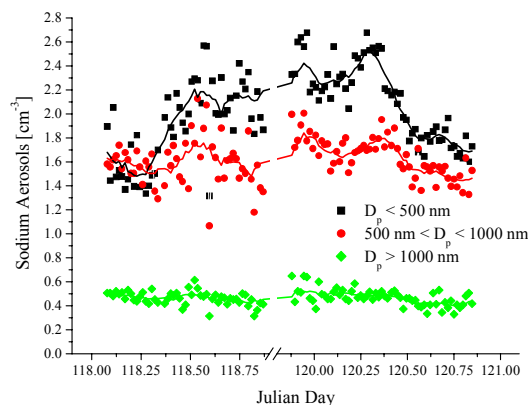


Figure 8: Number of sodium containing aerosols measured per 20 min sampling cycle over the 48 h measurement period at SEAS, broken down by equivalent size. Between JD 117.9 and JD 118.07 there is no reliable calibration.

The equivalent NaCl aerosol diameters, calculated using a density of 2.1, were converted into a 25 “channel” aerosol number distribution with a step width, $d\log D_p = 0.05$. This number of bins seemed to be the best compromise between resolution and optimizing counting statistics. Fig. 7 shows such a calculated distribution for a typical sodium mass data set. It also shows the impact of uncertainties in the sodium mass calibration for a worst case scenario. The statistical calibration error is around $\pm 6\%$, the 20% mass calibration uncertainty shown in the figure reflects the variation of calibration results over a year of measurements including two complete realignments. It translates on average to a 10 to 20% error for $dN/d\log D_p$, except at the edges of the distribution as discussed below.

Overall, most distributions were fairly similar to the one shown, with statistical errors on the order of

10 –20%. In order to discern trends, we examined the temporal variability of a three bin distribution (<500 nm, 500 to 1000 nm, >1000 nm) for all 123 available data sets, as shown in Fig. 8. The concentrations of aerosols bigger than 500 nm remained nearly constant over the course of the two days. This was expected as most of those particles came from sea spray and wind speeds were fairly constant. We saw no tidal dependency in particle concentration. Aerosol particle concentrations dropped twice in response to rain events, on JD 118.6 and JD 118.82, in all sizes ranges. Total particle concentrations below 500 nm increased starting around JD 118.3 and remained at higher levels until the last third of the second day of measurements. This most likely reflects the reported post-frontal change in air mass during JD 118.

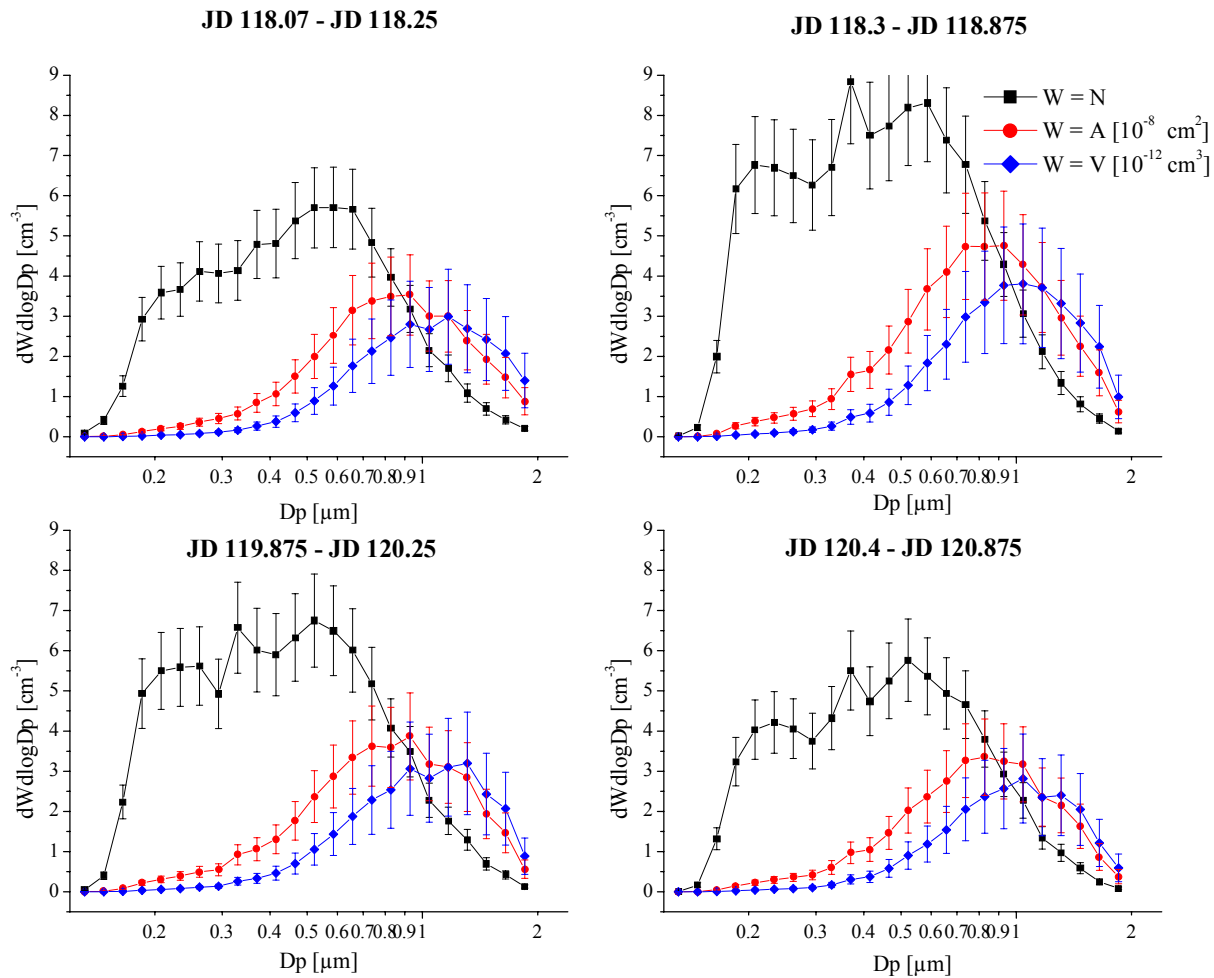


Figure 9: Averages for $dN/d\log D_p$, $dA/d\log D_p$ and $dV/d\log D_p$ for sodium containing particles during the four time periods shown in Figure 8. Particle diameters are equivalent dry sodium diameters.

Based on the preliminary trends in the sub 500 nm range, the data was subdivided into four time periods: JD 118.07 –118.25 (pre-front), JD 118.3–118.75 (new airmass, rain events were stripped), JD 119.875–120.25 (same aerosol count, one day later) and JD 120.4–120.875 (smaller aerosol load). For each time period, all sodium masses were aggregated into one data set and one size distribution generated as described. Errors resulted from the statistical counting error and the calibration error ($\pm 15\%$). Area and volume distributions were also calculated from the number distribution using average diameters. Fig. 9 shows the resulting distributions.

5. DISCUSSION

The distributions from Fig. 9 all show a steep decline below 210 nm which is due to aerosol undercounting around the triggering threshold and a conservative discrimination against small potentially spurious emission signals during raw data analysis. Above 1.1 μm , on the other hand, both the volume and area distributions seem to fall off short of the expected mode maximum for seasalt around 3 μm (Clarke et al, this issue). This is somewhat lower than the 2.0–2.5 μm cut-off that the transmission measurements with VOAG aerosols suggest, but, as size was not monitored separately, this might well be due to issues such as the lower density of seasalt vs. pure NaCl dried aerosols, longer drying times or the presence of other salts. This would lead in all cases to a bigger particle diameter at the same equivalent NaCl diameter and hence, lower transmission.

Because the ASD operated in an unsized mode, i.e. without a DMA for size segregation, the distributions shown in Fig 9 are plotted as equivalent dry sodium diameters. Hence the sodium signal could, in principle, arise from an internally mixed aerosol of larger diameter with a fractional sea salt composition. However, as we discuss below, Fig. 10 shows that the ASD distributions are in good agreement with the refractory i.e. sea salt distributions obtained by the OPC in clean air, particularly above 700 nm. This correlation of OPC refractory particle counts, with the ASD distributions suggests that the amount of internally chemically mixed aerosols was low and that the ASD distributions shown in Fig. 9 represent particles that consist largely of seasalt. The number distributions change with time increasing during the second half of the first measurement period corresponding to an increase in wind speed. We find the number distributions peaking at 500 nm. In all four cases we measure sub-micrometer sea salt down to our current detection limit of 200 nm.

6. COMPARISON WITH OPC DATA

The SEAS experiments offered the opportunity to compare the ASD measurements with heated OPC measurements. In the OPC system ambient particle counts are compared with those obtained after heating the particles to 300 °C. It is assumed that all volatile components such as water and sulfate are removed and a size distribution of the non-volatile components such as sea salt and dust can be obtained. Since the ASD operated in a non size-resolved mode, comparison with size-resolved distributions is essential for the interpretation of our data.

The OPC data were averaged over the same time periods used to analyze the ASD data. No measurements are available for most of JD 119, so no comparison could be drawn for this time period. Fig. 10 compares the averages of the unheated (50 °C) and heated (300 °C) OPC distributions with our data for the first time periods.

There is fair agreement between the heated OPC distribution and the ASD data between 500 and 2000 nm. The fine structure at 750 nm in the OPC distribution is not real aerosol structure but is caused by Mie oscillations. The ASD appears to under-count particles with diameters >1100 nm but counting statistics are poor. However, both data sets agree within error limits; an agreement that, considering the assumptions involved in the calculation of the ASD distributions, is quite remarkable. As noted above, most particles in this range seem to be 100% sea salt.

Between 250 and 500 nm, the agreement is again reasonable for this period when we sampled clean air. It suggests that the heated OPC measurements reliably reflect the sea salt distribution in the absence of significant concentrations of mineral dust aerosols. It further indicates that sulfate aerosol particles are the dominant constituent of the total aerosol distribution in this diameter range. Fig. 11 shows the comparison for two periods after the passage of the front. During this period the ASD counts are lower than the refractory OPC counts. The agreement is particularly poor below 500 nm, when the OPC counted up to 5 times more aerosols at 250 nm. Interpretation of this data is clearly complicated by the fact that the ASD operated in an unresolved sizing mode.

However, we believe these differences are real and that the two instruments were measuring aerosol particles of different chemical composition. The most obvious explanation is that after the frontal passage the air mass contained a substantial fraction

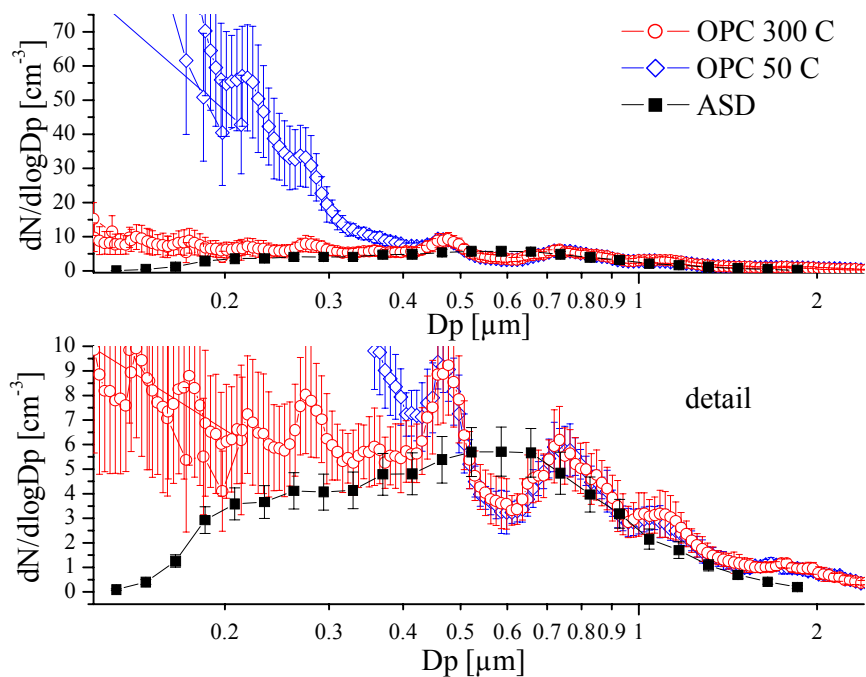


Figure 10: Comparison of the average ASD size distributions (i.e. equivalent geometric diameter of dry sea salt) with the average of the OPC distributions for the unpolluted time period (JD 118.07-118.25), taken 2 m below the ASD inlet, after heating the aerosols to 50 respectively 300 C (cf. Clarke et al, this issue).

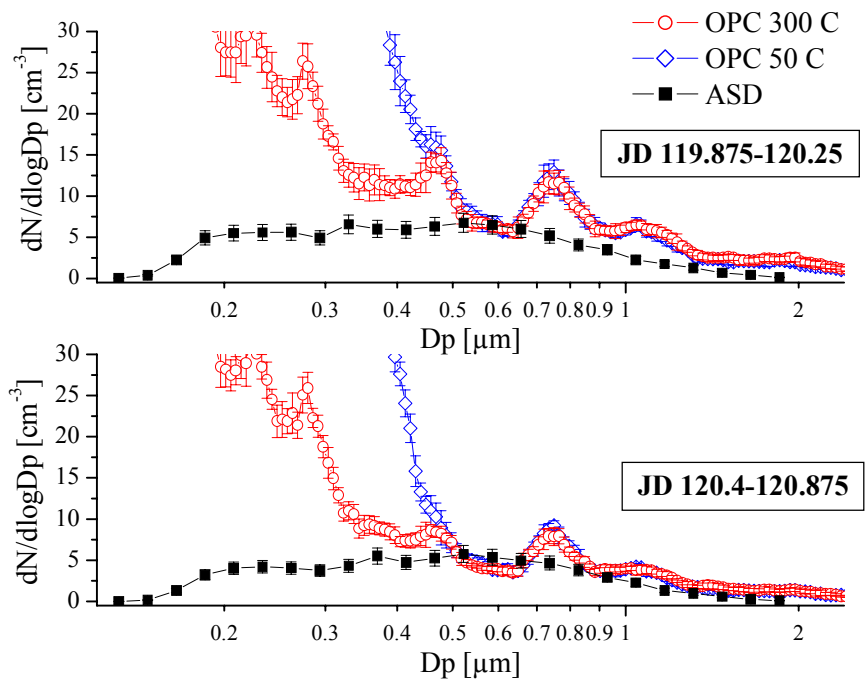


Figure 11: As Figure 10, for the second day of measurements.

of refractory small particles that were not composed primarily of sea salt.

There is some evidence for this in light absorption measurements (Masonis et al., this issue) and in refractory CN number for this period (A. Clarke personal communication). Without measurements of the chemical composition of these aerosols it is not possible to definitively determine the source of this discrepancy.

7. CONCLUSION

The measurements reported here represent the first field deployment of the ASD and demonstrated that it is capable of providing an extensive data set of sea salt distributions which are quantitative and have high temporal resolution. The opportunity to deploy the instrument as part of a field campaign focusing exclusively on aerosol particle measurements was invaluable, particularly the opportunity to compare with a heated OPC instrument. We obtained reasonable agreement between the instruments when sampling in clean air,

8. REFERENCES

Berglund, R. N. and B. Y. H. Liu (1973). "Generation of Monodisperse Aerosols." Environmental Science and Technology **7**(2): 147-153.

Charlson, R. J., J. E. Lovelock, M. O. Andreae and S. G. Warren (1987). "Oceanic phytoplankton, atmospheric sulfur, cloud albedo and climate." Nature **326**(6114): 655-661.

Charlson, R. J., S. E. Schwartz, J. M. Hales, R. D. Cess, J. A. Coakley, J. E. Hanson and D. J. Hoffman, (1992) "Climate forcing by anthropogenic aerosols" Science, **255** (5043): 423-430.

Clark, C. D., P. Campuzano-Jost, D. S. Covert, R. C. Richter, H. Maring, A. J. Hynes and E. S. Saltzman (2001). "Real-time measurement of sodium in single aerosol particles by flame emission: laboratory characterization." J. Aerosol. Sci. **32**(6): 765-778.

Clarke, A.D. (1991) "A Thermo-optic technique for in-situ analysis of size-resolved aerosol physicochemistry", Atmos. Env., **25A**, 3/4, 635-644, 1991

Clarke, A.D. and J.N. Porter,(1993) "Pacific marine aerosol Part II: Equatorial gradients, ammonium and chlorophyll during SAGA3", J. Geophys. Res., **98**, 16,997-17,010.

validating the ASD and demonstrating that aerosol volatility measurements can provide reliable sea salt distributions. The combination of these measurements indicates that seasalt was the dominant constituent of aerosol particles with diameters larger than 500 nm and that sulfate was the dominant constituent at smaller diameters.

There were significant differences in measurements by the two instruments after the passage of a front that brought a polluted air mass into the site, suggesting that the instruments were measuring different things. One possible explanation is the presence of refractory aerosol particles of anthropogenic origin, however size resolved measurements from the ASD would do much to illuminate the origin of this discrepancy.

Acknowledgements

This work was funded by the Office of Naval Research (Grant No. N0001499-1-0031)

Guazzotti, S. A., K. R. Coffee and K. A. Prather (2001). "Continuous measurements of size-resolved particle chemistry during INDOEX-Intensive Field Phase 99." J. Geophys. Res.-Atmos. **106**(D22): 28607-28627.

Hobbs, P. V. (1971). "Simultaneous airborne measurements of cloud condensation nuclei and sodium containing particles over the ocean." Quarterly Journal of the Royal Meteorological Society **97**: 263-271.

Meszaros, A. and K. Vissy (1974). "Concentration, Size Distribution and Chemical Nature of Atmospheric Aerosol Particles in Remote Oceanic Areas." Aerosol Science **5**: 101-109.

Murphy, D..M., J. R. Anderson, P. K.Quinn, L. M.. McInnes, F. J. Brechtel, S. M. Kreidenweis, A. M. Middlebrook, M. Posfai, D. S. Thomson, and P. R. Bruseck, (1998). Influence of sea-salt on aerosol radiative properties in the Southern Ocean marine boundary layer. Nature, **392**: 62-65.

O'Dowd, C. D., J. A. Lowe and M. H. Smith (1999). "Coupling sea-salt and sulphate interactions and its impact on cloud droplet concentration predictions." Geophys. Res. Lett. **26**(9): 1311-1314.

O'Dowd, C. D., M. H. Smith, I. E. Consterdine and J. A. Lowe (1997). "Marine aerosol, sea-salt, and the marine sulphur cycle: A short review."

Atmos. Environ. **31**(1): 73-80.

- O'Dowd, C. D. M. H. Smith and S. G. Jennings, (1993) "Physico-chemical properties of aerosol over the north east atlantic: Evidence for wind speed related sub-micron sea salt aerosol production" J. Geophys. Res. **98**, 1137-1149.
- Pilinis, C., S. N. Pandis and J. H. Seinfeld (1995). "Sensitivity of direct climate forcing by atmospheric aerosols to aerosol-size and composition." J. Geophys. Res.-Atmos. **100**(D9): 18739-18754.
- Prospero, J. M. (2002) "The chemical and physical Properties of Marine Aerosols: An Introduction" "Advances in Marine Biogeochemistry" Springer-Verlag. in press.
- Radke, L. F. and P. V. Hobbs (1969). "Measurement of Cloud Condensation Nuclei, Light Scattering Coefficient, Sodium-Containing Particles, and Aitken Nuclei in the Olympic Mountains in Washington." J. Atmos. Sci. **26**: 281-288.
- Satheesh, S. K., V. Ramanathan, L. J. Xu, J. M. Lobert, I. A. Podgorny, J. M. Prospero, B. N. Holben and N. G. Loeb (1999). "A model for the natural and anthropogenic aerosols over the tropical Indian Ocean derived from Indian Ocean Experiment data." J. Geophys. Res.-Atmos. **104**(D22): 27421-27440.
- Tang, I.N., (1997), "Thermodynamic and optical properties of mixed -salt aerosols of atmospheric importance", J. Geophys. Res.-Atmos. **102**(D2): 1883-1893.
- Weis, D. D. and G. E. Ewing (1999). "Water content and morphology of sodium chloride aerosol particles." J. Geophys. Res.-Atmos. **104**(D17): 21275-21285.
- Westenberger, S., T. Heibel, J. Gebhart and C. Roth (1990). "Continuous Monitoring of Droplet Production of a Vibrating Orifice Generator By Laser-Light Extinction." J. Aerosol. Sci. **21**: S547-S550.